Received: 20 December 2019 | Revised: 7 May 2020 | Accepted: 4 July 2020

DOI: 10.1002/jcc.26387

FULL PAPER

Journal of COMPUTATIONAL CHEMISTRY WILEY

Potential energy function for a photo-switchable lipid molecule

Oskar Klaja[1] | James A. Frank[2] | Dirk Trauner[3] | Ana-Nicoleta Bondar[1]

[1]Department of Physics, Theoretical Molecular Biophysics Group, Freie Universität Berlin, Berlin, Germany

[2]Vollum Institute, Oregon Health & Science University, Portland, Oregon

[3]Department of Chemistry, New York University, New York, New York

Correspondence
Ana-Nicoleta Bondar, Department of Physics, Theoretical Molecular Biophysics Group, Freie Universität Berlin, Arnimallee 14, D-14195 Berlin, Germany.
Email: nbondar@zedat.fu-berlin.de

Funding information
Deutsche Forschungsgemeinschaft, Grant/Award Number: SPP1926; Excellence Initiative of the German Research Foundation, via the Freie Universität Berlin.

Abstract

Photo-switchable lipids are synthetic lipid molecules used in photo-pharmacology to alter membrane lateral pressure and thus control opening and closing of mechanosensitive ion channels. The molecular picture of how photo-switchable lipids interact with membranes or ion channels is poorly understood. To facilitate all-atom simulations that could provide a molecular picture of membranes with photo-switchable lipids, we derived force field parameters for atomistic computations of the azobenzene-based fatty acid FAAzo-4. We implemented a Phyton-based algorithm to make the optimization of atomic partial charges more efficient. Overall, the parameters we derived give good description of the equilibrium structure, torsional properties, and non-bonded interactions for the photo-switchable lipid in its *trans* and *cis* intermediate states, and crystal lattice parameters for *trans*-FAAzo-4. These parameters can be extended to all-atom descriptions of various photo-switchable lipids that have an azobenzene moiety.

KEYWORDS

cis-azobenzene, force-field, photo-switchable lipids, potential energy function, trans-azobenzene

1 | INTRODUCTION

Photo-pharmacology is an emerging field that uses drug molecules whose biological action can be controlled with light.[1] Prominent examples include photo-switchable ion-channel blockers to restore vision in mice,[2] a photo-switchable antidiabetic drug, glimepiride, to control insulin release,[1,3] and a photo-switchable capsaicin mimic as pain medicine.[4]

An important class of photo-switchable compounds are photo-switchable lipids, synthetic lipid molecules that have an alkyl chain replaced by an azobenzene moiety.[1,4,5] The light-induced isomerization from *trans* to the *cis* isomer of a photo-switchable lipid (Scheme 1) can be exploited to alter the lateral membrane pressure and thus control the opening and closing of mechanosensitive ion channels.[4,5] The molecular picture of how photo-switchable lipids interact with membranes is largely unclear.[6,7] To enable numerical simulations of membranes with photo-switchable lipids, we derived CHARMM (Chemistry at Harvard Molecular Mechanics[8]) force-field parameters for an azobenzene-based photo-switchable lipid.

The photo-switchable lipid we parametrized is a photo-switchable fatty acid analogue coined FAAzo-4. It is composed of azobenzene substituted with butyl and butanoic acid in its 4 and 4′ positions[4] (Scheme 1). An important advantage in using FAAzo-4 as model system to parametrize a photo-switchable lipid is that the three-dimensional structure of *trans*-FAAzo-4 has been solved by X-ray crystallography at high-resolution.[4] There are 4 *trans*-FAAzo-4 molecules in one unit cell (Figure S1a), arranged such that their carboxylic acid groups hydrogen bond to each other (Figure S1c). The two benzene rings are almost co-planar, with the central N1═N2 bond in a *trans* geometry (Figure 1a) and the two benzene rings slightly tilted such that the N2═N1—C9—C10 and N1═N2—C3—C8 dihedral angles (Figure 1a) are −1.5° and −2.1°, respectively (Figure 1). The almost

co-planar geometry of the two benzene rings in the crystal structure (Figures S1–S3) is consistent with earlier predictions from ab initio computation.[9]

Understanding how azobenzene-based lipids interact with membranes, and how membrane properties change in the presence of azobenzene-based lipids, is important for the design of new photo-switchable lipids with tailored physical–chemical properties. Presence of azobenzene-substituted pentyl phosphate (4-Azo-5P) in a membrane led to lower acyl lipid order parameters[5]; the *trans*-isomer of 4-Azo-5P associated with larger anisotropy and compressibility of the area as compared to *cis*.[5] The *trans-cis* photoisomerization of photo-switchable lipids can be used to alter the local fluidity of a membrane[10] and the shape of unilamellar vesicles.[6]

Computer simulations are a valuable approach to characterize the properties of lipid bilayers with photo-switchable lipids, because they allow us to model lipid membranes of various compositions and to explore the dynamics and molecular interactions of each of the components of the membrane system. The simulations involve solving numerically classical mechanical equations of motion for all atoms of the system, and then generating a molecular dynamics trajectory that describes the time-evolution of the atomic coordinates. Interactions between atoms of the system are described by a potential energy function that depends on the atomic coordinates of the system being studied, and on parameters—denoted force-field parameters, typically derived based on quantum mechanical (QM) computations. These parameters ensure that the structure and energetics of the system are properly described with the molecular mechanics (MM) force field computations.

MM force fields contain parameters for numerous types of lipid molecules. However, photo-switchable lipids are novel molecules that to date, lack an accurate atomistic force-field representation. Such a representation would require proper description of the azobenzene moiety, and of the bonded and non-bonded interactions between the azobenzene moiety and the remainder of the lipid molecule (Scheme 1).

The isolated azobenzene moiety and several azobenzene derivatives are represented in the Universal Force Field (UFF[11]) and the Polymer Consistent Force Field (PCFF[12,13]). These force fields can treat liquids and polymers, but are not optimized for simulations of biomolecular systems that include proteins. A coarse grain description of azobenzene was derived for MARTINI,[14] and a reactive force-field was derived for ReaxFF.[15] Several degrees of freedom of the azobenzene moiety were parametrized for AMBER: The dihedral angle that describes the twist of the benzene rings about the central N1═N2 double bond was parametrized using B3LYP/6-31G*,[16] and the C9—N1═N2—C3 and C9—N1═N2 dihedral angles (Scheme 1) were parametrized using Complete Active Space (CASSCF) computations.[17] A B3LYP-based AMBER

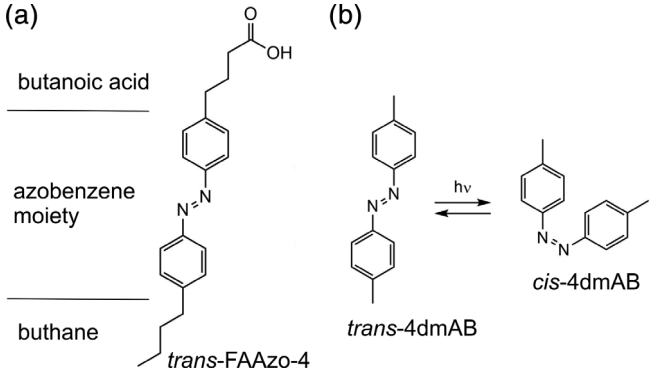

SCHEME 1 Molecular structure of FAAzo-4 and isomeric states of 4dmAB. (a) Molecular structure of *trans*-FAAzo-4. (b) Schematic representations of *trans*-4dmAB and *cis*-4dmAB

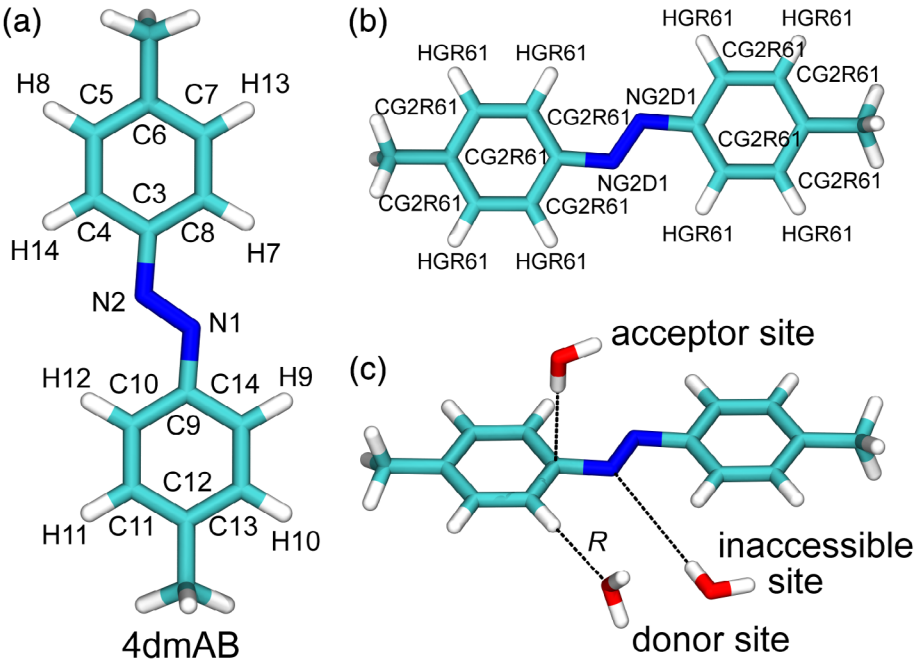

FIGURE 1 Atom names and water interaction sites. (a) Molecular structure of *trans*-4dmAB with CHARMM atom names. (b) Molecular structure of *trans*-4dmAB with CHARMM (CGenFF) atom types. (c) Schematic representation of donor and acceptor sites of 4dmAB used to compute ΔE and R values [Color figure can be viewed at wileyonlinelibrary.com]

parametrization for 4-hydroxy-4′-methyl-azobenzene[18] relied on atomic partial charges from electrostatic potential fitting (EPS). On the 4-OH-substituted benzene ring of this molecule, the charges for C and H atoms close to hydroxyl oxygen atom differ from those found on the unsubstituted benzene ring where C and H are close to 4′-methyl group. Description of azobenzene with alkyl-substitutions, as in FAAzo-4, might thus be difficult with this set of AMBER parameters.

Relatively recently, a set of CHARMM force field parameters was presented for azobenzene in McCullagh et al.[19,20] Atomic partial charges for azobenzene atoms were derived from ESP computations,[19] whereas for the internal consistency of CHARMM it is recommended that partial charges be derived by fitting to Hartree-Fock (HF) computations of water interaction energies.[21] Bonded parameters involving the nitrogen atoms (Scheme 1) were taken from parameters involving nucleic acid aromatic carbon, without further revision.[19]

To enable reliable atomistic simulations of lipid membranes with photo-switchable lipids, we present here a complete set of CHARMM-compatible parameters for FAAzo-4 (Scheme 1). We used the CHARMM General Force Field (CGenFF) protocol[21] for the parametrization of drug-like molecules in CHARMM. In this protocol, MM charges are optimized by fitting to QM computations of water interaction energies and distances, and parameters for bonded degrees of freedom by fitting to QM computations of potential energy scans.[21] We obtained a good description of the geometry and water interactions of FAAzo-4 and of the crystal lattice from X-ray crystallography. The parameters we derived for FAAzo-4 can be transferred to the CHARMM parametrization of other azobenzene moieties with alkyl substitutions at positions 4- and 4′.

2 | METHODS

2.1 | Protocol used for deriving CHARMM force-field parameters

The empirical CHARMM MM force field equation[8] includes terms for bonded and non-bonded interactions as follows:

$$\begin{aligned} V(R) = &\sum\nolimits_{\text{bonds}} k_b(b-b_0)^2 + \sum\nolimits_{\text{angles}} k_\theta(\theta-\theta_0)^2 \\ &+ \sum\nolimits_{\text{dihedrals}} k_\varphi[1+\cos(n\varphi-\delta)] \\ &+ \sum\nolimits_{\text{impropers}} k_\omega(\omega-\omega_0)^2 + \sum\nolimits_{\text{Urey-Bradley}} k_{UB}(u-u_0)^2 \\ &+ \sum\nolimits_{i,j} \frac{q_i q_j}{4\pi\epsilon_0\varepsilon r_{ij}} + \sum\nolimits_{i,j} \epsilon_{ij}\left[\left(\frac{R_{\min,ij}}{r_{ij}}\right)^{12} - 2\left(\frac{R_{\min,ij}}{r_{ij}}\right)^{6}\right] \end{aligned} \quad (1)$$

where k_b and k_θ are force constants for the harmonic terms describing bond stretching and valence angle bending, respectively; b_0 and θ_0 are the equilibrium values for these terms. Dihedral angles φ are given as a sum of cosine functions with k_φ—the force constant, n—the multiplicity, with integer values between 1 and 6, and δ—the phase shift.[8] Improper angles can be used to control chirality and planarity.[8] Non-bonded interactions between two atoms i and j separated by the distance r_{ij} include electrostatic interactions between two atomic partial charges q_i and q_j, and van der Waals interactions characterized by the minimum interaction distance $R_{\min,ij}$, and the well depth ε_{ij}.[8] In addition to the terms given by Equation (1), CHARMM includes the CMAP correction for the protein backbone.[22]

To be consistent with the CHARMM force field, parameters for a non-standard molecule such as a photo-switchable lipid would need to be derived according to the CGenFF protocol for drug-like molecules.[21] This protocol involves QM geometry optimizations of the target molecule, optimizations of the atomic partial charges, and an iterative procedure to optimize bonded parameters.[21]

The optimization of atomic partial charges relies on computations of water interaction energies and distances with QM and MM. Here, the water interaction energy ΔE is defined as the difference between the energy of an azobenzene molecule and a water molecule (Figure 1c), and the sum of the energy $E(azobenzene)$ of the isolated azobenzene molecule and that of the energy $E(water)$ of an isolated water molecule:

$$\Delta E = E(\text{azobenzene} + \text{water}) - [E(\text{azobenzene}) + E(\text{water})] \quad (2)$$

The water interaction distance R is the optimal interaction distance between the oxygen/hydrogen atom of the water molecule and the hydrogen or heavy atom of the azobenzene molecule (Figure 1c). ΔE and R are computed with internally fixed geometries of the azobenzene and water molecules. We used an azobenzene structure optimized with MP2/6-31G*; as recommended in the CGenFF protocol,[21] for the water geometry we used TIP3P.[23]

The target QM values ΔE_{QM} and R_{QM} for all water-accessible donor and acceptor sites are computed first with HF/6-31G*[21]; MM values ΔE_{MM}, and R_{MM} are then calculated, and partial atomic charges of the target molecule are adjusted manually until ΔE_{MM} and R_{MM} agree with the corresponding QM target values for all sites.[21] For neutral polar compounds, as is the case of the azobenzene moiety we parametrized here, ΔE_{MM} values are scaled by 1.16, and R_{MM} values are offset by –0.2 Å.[21]

Optimization of the partial atomic charges is considered converged when ΔE and R computed with MM versus QM agree to within 0.2 kcal/mol and 0.2 Å, respectively.[21] For weak interactions, a less restrictive converge criterion of 0.5 kcal/mol can be used.[21]

2.2 | Identifying parameters of FAAzo-4 that require optimization

To identify the CHARMM force field parameters that need to be refined for describing FAAzo-4, we used ParamChem[24] to search for parameters based on similarity to other molecules included in CGenFF. ParamChem searches for parameters and provides penalty scores that indicate the accuracy of the existing CHARMM parameters in describing the target molecule. A penalty score of zero indicates a good description of that particular degree of freedom,

whereas a score >10 for a parameter indicates a poor force-field description.

Our ParamChem search indicated that the butyl and butanoic acid moieties of FAAzo-4 (Scheme 1) are well described by CGenFF, with penalty scores close to 0. Likewise, ParamChem indicated reasonable description for the partial atomic charges of carbon atoms distant from the central double bond (penalty score of 6 for C5, C7, C11, C13 in Figure 1a). In contrast, the partial atomic charges of atoms close to the central double bond (atoms C4, C8, C10, C14 in Figure 1a) had a score of 10, carbon atoms directly bonded to N1 and N2 a score of 127, and the partial atomic charges for N1 and N2 had a score of 139. All bonded and non-bonded parameters involving N1 and N2 and the four carbon atoms directly bonded to the nitrogen atoms (C4, C8, C10, C14 in Figure 1a) had scores >10. A summary of the bonded parameters with high ParamChem scores is presented in Tables 1 and 2.

Pursuant to the observations above, we proceeded to optimize bonded parameters for the linkage region of 4,4′-dimethylazobenzene, and the partial atomic charges of the molecule. For the parametrization, we used the core structure of FAAzo-4, 4,4′-dimethylazobenzene (Scheme 1). For simplicity, in what follows we denote 4,4′-dimethylazobenzene as 4dmAB (Scheme 1, Figure 1a).

TABLE 1 Summary of bonded parameters optimized for *trans*-4dmAB

Atom names						
Bonds				k_b (kcal/mol/Å^2)	b_0 (Å)	
N1	N2			700	1.26	
N2	C3			305	1.41	
Valence angles				k_θ (kcal/mol/rad^2)	θ_0 (°)	
N2	C3	C4		40	120	
N1	N2	C3		80	104.8	
Dihedral angles				k_φ (kcal/mol)	n	δ (°)
C9	N1	N2	C3	15.20	2	180
C9	N1	N2	C3	0.50	4	0
N1	N2	C3	C4	2.70	2	180
N1	N2	C3	C4	0.25	4	0
N2	C3	C4	C5	6.50	2	180
N2	C3	C4	C5	0.80	4	0

Note: The parameters are introduced in Equation (1). Atom labels are presented in Figure 1. All values reported in the table are MM-optimized parameters for bonded interactions.

2.3 | Starting coordinates for 4dmAB in *trans* and *cis* isomeric states

The high-resolution crystal structure[4] was used for the starting coordinates of *trans*-FAAzo-4. The 4dmAB core moiety was prepared by replacing the sidechains of *trans*-FAAzo-4 with methyl groups using Avogadro.[25] The *cis* geometry of 4dmAB was prepared by editing *z*-matrix in Molden[26] to set the dihedral angles C9—N1═N2—C3 and N1═N2—C3—C8 (Figure 1) to 8° and 56° respectively.[27]

2.4 | Geometry optimizations with QM

For all QM computations we used Gaussian09[28] with standard convergence criteria. Our choice of MP2 for all QM geometry optimizations is based on tests indicating that MP2 allows us to reproduce the geometry of the *cis*-azobenzene fragment used for parametrization. As a reference for the geometry of the *cis*-azobenzene fragment we used the crystal structure from Mostad and Rømming.[27]

TABLE 2 Summary of bonded parameters optimized for *cis*-4dmAB

Atom names						
Bonds				k_b (kcal/mol/Å^2)	b_0 (Å)	
N1	N2			785	1.24	
N2	C3			245	1.41	
Valence angles				k_θ (kcal/mol/rad^2)	θ_0 (°)	
N2	C3	C4		24	130	
N1	N2	C3		55	95	
Dihedral angles				k_φ (kcal/mol)	n	δ (°)
C9	N1	N2	C3	18.10	2	180
C9	N1	N2	C3	0.30	4	0
N1	N2	C3	C4	1.80	2	180
N1	N2	C3	C4	0.13	4	0
N2	C3	C4	C5	5.60	2	180
N2	C3	C4	C5	0.80	4	0

Note: All values reported in the table are MM-optimized parameters for bonded interactions.

2.5 | Water interaction energy and distances and an automated protocol to optimize partial atomic charges

We used the ForceField Toolkit[29] of Visual Molecular Dynamics (VMD[30]) to generate starting geometries for the MP2-optimized structure of 4dmAB and water at 22 interaction sites (Figure 1c). To calculate ΔE and R we used the parametrization scripts from the webpage of Prof. Alexander MacKerell Jr. at the University of Maryland, USA.

To make the charge optimization step more efficient, we implemented a Phyton script that uses CHARMM to compute optimal values for R and ΔE, and Sequential Least Squares Programming (SLSQP[31]) in the SciPy Python library to optimize the partial atomic charges; the optimization of the charges was done in an outer Python loop that uses the *multiprocessing* Python library. The squared differences in ΔE and R obtained from the CHARMM calculation were used as a penalty function that is a subject to minimization with a convergence criterion of $1e^{-6}$.

Test computations indicated that when 4dmAB is *trans*, atoms N1 and N2 (Figure 1a) are poorly accessible to water, and we could not obtain convergence of the partial atomic charges for these two atoms. For example, when we attempted to probe water interactions at N1 with the water molecule placed such that its hydrogen-bonding OH bond was perpendicular to the plane of the benzene ring, strong interactions between the water molecule and N2 hindered convergence of the QM computations. Likewise, when we probed water interaction such that the OH bond of the water molecule was parallel to the plane of the benzene rings (Figure 1c) the repulsion from H7 or H12 atoms of 4dmAB would not allow the water molecule to hydrogen bond to N1 or N2 (Figure 2, Table 3).

Since *cis*-4dmAB allows water to access the central double bond of the molecule and does not deviate strongly from *trans*-4dmAB charges (Table S1), we used this geometry to optimize all partial atomic charges.

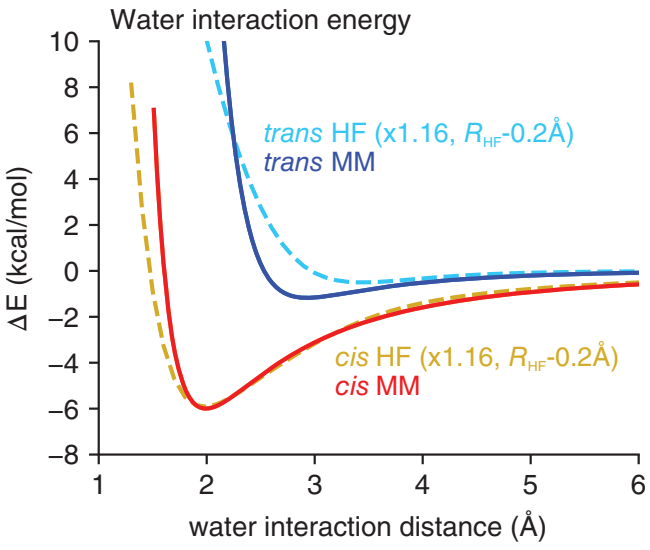

FIGURE 2 Scan of water interaction energies for atom N1 of *trans*-4dmAB versus *cis*-4dmAB computed with HF/6-31G* and with the MM parameters derived here. The nitrogen atoms of azobenzene moiety are significantly less accessible to water in *trans*-4dmAB than in *cis*-4dmAB. With HF, which is used for optimization of charges according to CGenFF protocol, interaction of *trans*-4dmAB with water is very weak (−0.4 kcal/mol). Note that the HF water interaction energies were scaled by 1.16 and interaction distances offset by −0.2 Å, as required by the CGenFF protocol for neutral polar compounds [Color figure can be viewed at wileyonlinelibrary.com]

2.6 | Choice of the van der Waals parameters

ParamChem assigned to the carbon and hydrogen atoms of azobenzene standard van der Waals parameters for benzene rings. In what follows, these standard van der Waals parameters are denoted as Set-1 (Table 4).

All our attempts to optimize partial atomic charges of *cis*-4dmAB with van der Waals parameters Set-1 failed to give ΔE_{MM} and R_{MM} values within acceptable convergence criteria. To circumvent this problem, we used the van der Waals parameters used in CGenFF for aromatic ring hydrogen atoms adjacent to highly polarized heteroatoms such as nitrogen atoms. These van der Waals parameters are denoted here as Set-2 (Table 4).

2.7 | Optimization of the torsional potential for the central N1═N2 double bond

Test computations with MP2/6-31G* indicated that twisting the N1═N2 bond of *trans*-4dmAB to 50° costs ~20 kcal/mol (Figure S4).

TABLE 3 Water interactions of the N1 and N2 atoms of FAAzo-4 computed with MM

FAAzo-4 isomer	ΔE (kcal/mol)	R (Å)
cis	−5.9	2.2
trans	−0.4	3.6

Note: We report water interaction energies computed with HF/6-31G*, and the corresponding water interaction distances.

TABLE 4 Summary of parameter sets derived for *trans*- and *cis*-FAAzo-4

Parameter set	Conformation	Van der Waals[a]
Set-1	*trans*	Benzene
	cis	Benzene
Set-2	*trans*	NADP[b]
	cis	NADP

Note: The van der Waals parameters used for Set-1 and Set-2 are listed in Table S1.

[a]van der Waals parameters used for the hydrogen atoms of the benzene rings.

[b]Nicotine adenine dinucleotide phosphate.

The high-energy penalty associated with twisting the central double bond indicates that spontaneous *trans-cis* isomerization is highly unlikely in equilibrium simulations of membranes containing azobenzene-based lipids at room temperature, as aimed with the parametrization we perform here. Pursuant to these considerations, we focused our parametrization of the N1═N2 bond twist to a maximum of 50°.

2.8 | Derivation of parameters for bond stretching and valence angle bending

The initial bonded parameters obtained with ParamChem were tested and adjusted by performing three-point PES scans with MP2/6-31G*. This procedure, which is consistent with the CHARMM force field protocol,[32] allows parametrization of the quadratic bond and angle potentials by fitting linear functions given by energies computed for three values of the degree of freedom being parametrized: The value of the degree of freedom (bond or angle) at the geometry-minimized structure without any restraint, one value decremented relative to this optimum, and one value incremented relative to the optimum. Ideally, the incremented bond or angle values give energy differences of 1–3 kcal/mol relative to the energy-minimized structure.[32] PES profiles for bond stretching were computed with a step of 0.05 Å; for PES of valence angles we used a step of 4°. Bond lengths and equilibrium valence angles were fit to resemble MP2 or crystallographic structures.

2.9 | Crystal lattice simulation

To assess the usefulness of our parameters for describing equilibrium structures and inter-molecular interactions of FAAzo-4, we sought to use the parameters for simulations of the crystal unit obtained from X-ray experiments.[4] We first constructed coordinates for a crystal unit by using the crystallographic information file of the crystal structure of FAAzo-4[4] and the free version of Mercury, the Cambridge Crystallographic Data Center crystal structure visualization software.[33] We then used these coordinates to generate a system of 64 *trans*-FAAzo-4 molecules using the Super Cell Builder functionality of Avogadro.[25]

Crystal lattice simulations were performed using NAMD2[34,35] using settings adopted from Nemkevich et al.[36] The time step for all simulations was 1 fs. We used a switching potential between 10 and 12 Å, particle mesh Ewald[37,38] for long-range Coulomb interactions, a Langevin piston to keep the pressure to 1 bar, and a Nose-Hoover thermostat to keep the temperature to the experimental value of 100 K; the Langevin damping coefficient was set to 1 ps^{-1}. Following geometry optimization and heating, we performed production runs of 2 ns using the *NPT* ensemble and isotropic pressure coupling.

In a separate set of simulations we constructed a crystal lattice composed of 64 4dmAB molecules based on the 4dmAB X-ray diffraction data from Harada et al.[39] The simulations on the 4dmAB crystal were performed using the same protocol as described above for FAAzo-4, but the temperature was set to 296 K, to be consistent with experimental conditions.[39] Convergence of the simulations was assessed by monitoring the crystal lattice vectors.

2.10 | MM potential of mean force profiles

To verify the dynamics of isolated *cis*-4dmAB at room temperature, we performed prolonged MM simulations from which we calculated potential of mean force (PMF) profiles for selected dihedral angles of the molecules. The geometry of the isolated *cis*-4dmAB molecule was first geometry optimized with the MM parameters derived here. Molecular dynamics simulations were initiated by first heating the systems to 300 K, followed by equilibration with velocity rescaling for 500 ns, and then by a 5 μs production run. We used an integration step of 1 fs, and saved coordinates each 1 ps. From the simulation trajectory, we extracted the values of selected dihedral angles, and calculated histograms for these dihedral angles. We computed PMF profiles according to the equation

$$\mathrm{PMF} = -k_B T \cdot \ln(density) \tag{3}$$

where k_B is the Boltzmann constant, T is the temperature in Kelvin, and *density* is the normalized distribution of the values of the dihedral angle.

3 | RESULTS AND DISCUSSION

We derived CHARMM force-field parameters for 4dmAB in *trans* and *cis* isomeric states and used these parameters to parametrize the complete FAAzo-4 molecule (Figure 1, Scheme 1). In what follows, we describe the parametrization of the bonded and nonbonded interactions for *trans* and *cis*-4dmAB, and tests to validate the parametrization of FAAzo-4.

3.1 | QM geometry optimization of *trans* and *cis*-4dmAB

The MP2-optimized geometry of *trans*-4dmAB is very close to the starting crystal structure coordinates; the average root-mean-squared distance (rmsd) between the heavy atoms of the two structures is within 0.1 Å (Table 5). In the MP2-optimized structure, the N2—C3 bond has the same length as in the crystal structure, 1.4 Å; at 1.28 Å, the length of the N1═N2 bond in the MP2-optimized structure is within the 1.24–1.28 Å interval found in Böckmann et al.[41] from QM computations of azobenzene, and close to the 1.26–1.27 Å interval found from inspection of azobenzene-based molecular crystals.[39] The two benzene rings of the MP2-optimized *trans*-4dmAB structure are co-planar, which is compatible with previous QM computations on an isolated *trans*-azobenzene.[9]

TABLE 5 Geometry of *trans*-4dmAB in MM- and QM-optimized structures, and in crystal structures

		MM optimization		MM crystal[a]		X-ray crystallography			
Degree of freedom		Initial	Optimized	Crystal	QM	300K[b]	296 K[c]	90K[c]	100 K[d]
Bond length (Å)	N1═N2	1.29	1.27	1.26	1.28	1.25	1.27[e]	1.27[e]	1.25
	N2—C3	1.43	1.44	1.43	1.42	1.43	1.43	1.44	1.43
Valence angle (°)	N1═N2—C3	119.7	113.8	114.0	113.6	113.3	114.5	114.2	113.9
	N2—C3—C4	116.6	115.1	114.8	115.0	115.5	115.0	115.0	115.5
Dihedral angle (°)	C9—N1═N2—C3	179.9	180.0	179.8	180.0	180.0	180.0	180.0	179.6
	N1═N2—C3—C4	0.1	0.1	3.5	0.1	7.1	1.8	1.3	2.1
	N2—C3—C4—C5	180.0	180.0	179.6	179.9	179.5	179.5	179.5	179.6

Note: "MM initial" versus "MM optimized" indicate the starting CHARMM force field parameters versus the MM parameters optimized here.
[a]MM simulations of a *trans*-FAAzo-4 crystal using the optimized MM parameters.
[b]Crystal structure of *trans*-azobenzene.[40]
[c]Crystal structure of *trans*-4dmAB.[39]
[d]Crystal structure of *trans*-FAAzo-4.[4]
[e]The value of 1.27 Å was estimated based on crystal structures of azobenzene compounds.[39]

TABLE 6 Geometry of *cis*-4dmAB optimized with MM versus MP2/6-31G*, and in the crystal structure

Degree of freedom		MM initial	MM optimized	QM	X-ray[a] 273 K
Bond (Å)	N1═N2	1.30	1.27	1.27	1.25
	N2—C3	1.43	1.44	1.44	1.44
Angle (°)	N1═N2—C3	123.4	121.6	121.2	121.9
	N2—C3—C4	118.4	117.4	116.8	117.3
Dihedral angle (°)	C9—N1═N2—C3	4.6	8.2	7.5	8.0
	N1═N2-C3—C4	58.8	54.7	53.6	56.3
	N2—C3—C4—C5	178.2	177.1	173.4	175.5

[a]Crystal structure of *cis*-azobenzene.[27]

In the MP2-optimized structure of *cis*-4dmAB, the length of the N1═N2 covalent bond is overestimated by 0.2 Å relative to the crystal structure[39] (Table 6); the N2—C3 bond length is the same as in the crystal structure.[39] The C9—N1═N2—C3 dihedral angle is within 1° from the corresponding crystal structure value, the N2—C3—C4—C5 and N1═N2—C3—C4 dihedral angles within ~3° (Table 6).

The MP2-optimized geometry of *cis*-4dmAB is compatible with previous ab initio computations on a *cis*-azobenzene indicating a small twist of ~0–11° around the central N1═N2 double bond.[9,41]

3.2 | Optimization of the partial atomic charges for *trans*- and *cis*-4dmAB

Based on considerations of water accessibility to the central N1═N2 double bond of 4dmAB (Table 3), we used the *cis* isomer for all water interaction energy computations and optimization of partial atomic charges. We performed two separate optimizations by using different van der Waals parameters for hydrogen atoms of the benzene rings (see Set-1 vs. Set-2 in Tables 4 and S2). Our strategy was to derive partial atomic charges that fit the CGenFF convergence criteria for water interaction energies (within 0.2–0.5 kcal/mol) and water interaction distances (within 0.2 Å).[21]

We initiated the optimization of partial atomic charges by including all atoms of the azobenzene moiety in the water interaction energy computations. As our test computations indicated poor convergence when attempting to re-compute all partial atomic charges, we reduced gradually the number of atoms whose partial atomic charges are allowed to vary; for atoms excluded from the charge optimization procedure we first used standard CHARMM partial atomic charges. These test computations led us to conclude that the CGenFF convergence criteria for water interaction energies are best met when only the partial atomic charges for N1, N2, C3, and C9 are optimized, and the partial atomic charges of atoms C6 and C12, which are zero in standard CHARMM, are set to 0.005*e*.

We found that the van der Waals parameters impact the description of the MM water interaction energies, and thus the convergence of the partial atomic charges. When using van der Waals parameters Set-1 (Tables 4 and S2) we obtained partial atomic charges that gave good description of ΔE and R for most of the heavy atoms of *cis*-4dmAB, but not for the hydrogen atoms. For example, for N1 and N2

TABLE 7 Water interaction energies and interaction distances for *trans*-4dmAB

	MP2		Set-1		Set-2	
Atom	ΔE	R	$\Delta\Delta E$	ΔR	$\Delta\Delta E$	ΔR
N1	−5.9	3.14	−0.1	0.0	−0.1	0.0
N2	−5.9	3.14	−0.1	0.0	−0.1	0.0
C3	−2.5	3.77	*−0.4*	−0.2	*−0.3*	−0.18
C9	−2.6	3.76	*−0.7*	−0.18	*−0.3*	−0.18
C4	−2.5	3.71	−0.1	−0.18	−0.1	−0.18
C14	−2.6	3.7	−0.1	−0.18	−0.2	−0.18
C8	−2.4	3.73	−0.0	−0.22	−0.1	−0.2
C10	−2.5	3.73	−0.1	−0.22	−0.1	−0.2
H7	−1.8	2.48	*−0.8*	0.36	−0.2	0
H12	−1.8	2.48	*−0.8*	0.36	−0.2	0
H9	−0.9	4.09	−0.2	−0.12	−0.1	−0.26
H14	−0.9	4.14	−0.2	−0.12	−0.1	−0.26
C5	−2.5	3.69	−0.2	−0.22	*−0.3*	−0.22
C13	−2.6	3.66	−0.2	−0.2	*−0.3*	−0.2
C7	−2.5	3.68	−0.2	−0.22	*−0.3*	−0.22
C11	−2.5	3.99	−0.2	−0.26	−0.3	−0.24
H8	−1.9	2.56	−0.4	0.3	−0.1	−0.04
H10	−1.9	2.56	*−0.4*	0.3	−0.1	−0.04
H11	−2.1	2.56	*−0.5*	0.3	−0.0	−0.04
H13	−2.1	2.55	*−0.5*	0.3	−0.0	−0.04
C6	−2.3	3.69	*−0.3*	−0.26	*−0.3*	−0.26
C12	−2.2	3.71	*−0.5*	−0.26	*−0.3*	−0.26

Note: ΔE_{QM} values were scaled by 1.16.[21] ΔE and $\Delta\Delta E$ values are reported in kcal/mol, and rounded up to the first decimal; and R and ΔR values in Å. Values in italics are larger than the CGenFF convergence criteria. Atom names are illustrated in Figure 1. Atomic partial charges optimized for Set-1 and Set-2 are presented in Table S3.

TABLE 8 Dipole moments computed for *cis*-4dmAB using MP2/6-31G* versus the MM parameters optimized here

	Dipole moment			
Method	*x*	*y*	*z*	Total
QM	−0.1	4.1	−0.0	4.1
MM	−0.0	4.8	0.0	4.8

Note: We report the *x*, *y*, and *z* components of the dipole moments, and the total dipole moment, in Debye, rounded up to the first decimal point. Computations were performed for geometries optimized with MP2 and, respectively, with MM.

ΔE converged to within −0.1 kcal/mol, whereas for most of the hydrogen atoms of *cis*-4dmAB the ΔE values computed with MM were within −0.3 to −0.8 kcal/mol from the corresponding QM target values (Table 7).

To improve the description of the partial atomic charges of *cis*-4dmAB, we used van der Waals parameters Set-2 (Tables 4 and S2). The agreement between ΔE_{QM} and ΔE_{MM} for all optimized sites improved to within −0.1 kcal/mol to 0.3 kcal/mol, and the R_{MM} values computed for all interaction sites of *cis*-4dmAB were within the convergence criteria (Table 7). Moreover, the partial atomic charges optimized with Set-2 allow good description of the molecular dipole moment of *cis*-4DmAb (Table 8): The dipole moment is overestimated by 17%, which is close to 20% overestimation recommended by the CGenFF protocol.[21]

3.3 | Optimization of bonded parameters for *trans*-4dmAB

The central N1═N2 bond of the azobenzene ring was absent from the result of our ParamChem search for force-field parameters. As a reference bond length for N1═N2 of *trans*-4dmAB we used 1.27 Å, which is close to the 1.28 Å value in the MP2-optimized structure, and to the 1.26–1.27 Å values from crystal structures[39] (Table 5). To ensure that the MM computations can give good agreement with MP2-optimized structures and with crystal structures (Table 5), we set the equilibrium distance for the N2—C3 bond to 1.44 Å; for the N1—N2—C3 and N2—C3—C9 valence angle values we decreased the equilibrium values from initial values of 120° and 116°, respectively, to 114° and 115°.

To evaluate the accuracy of the bonded parameters for bond stretching and valence angle bending, we performed three-point PES scans with MP2 and with MM. For the central N1═N2 double bond, we started by using the CGenFF force constant for a N═C bond with atom types NG2S1 and CG2R61 (500 kcal/mol/Å^2). Based on the PES computations, we increased this force constant to 700 kcal/mol/Å^2. For the N1═N2—C3 valence angle bending, we decreased the initial force constant from 100 kcal·mol^{-1}·rad^{-2} to 80 kcal·mol^{-1}·rad^{-2}, and obtained excellent agreement between MP2 and MM PES profiles (Figures 3 and S5).

We optimized three dihedral angles that include the N1 and/or N2 atoms of the central double bond: C3—N1═N2—C9, N1═N2—C3—C4, N2—C3—C4—C5, and monitored N2—C3—C4—H7 (Figures 1 and S4).

The dihedral angle C9—N1═N2—C3 describes the isomeric state of the molecule. Test computations indicated that the energy increases rapidly with twisting the N1═N2 double bond, such that in MP2 computations a twist of ~50° costs ~20 kcal/mol (Figure 4b). As we aim here to derive parameters to study the membranes with *trans*- or *cis*-FAAzo-4 close to the corresponding equilibrium structures, a description of highly twisted geometries close to the transition state for the isomerization is beyond the scope of our work. We thus restricted the parametrization of dihedral angles to torsions of up to 50°.

We obtained good agreement between the MP2 and MM PES for the C9—N1═N2—C3 dihedral angle by using two terms with multiplicities n = 2 and n = 4 (Figure 4b, Table 5). We used the same multiplicities to describe the torsional profile of the N1═N2—C3—C4 dihedral angle that describes rotation of the benzene rings around the N—C bond, and for the N2—C3—C4—C5 dihedral angle that describes bending of a benzene ring relative to the N1═N2 bond axis (Figures 4 and S4, Table 5). We found that the N2—C3—C4—H7 dihedral angle was well described once the torsional profiles mentioned above had been optimized, without the requirement of further optimization.

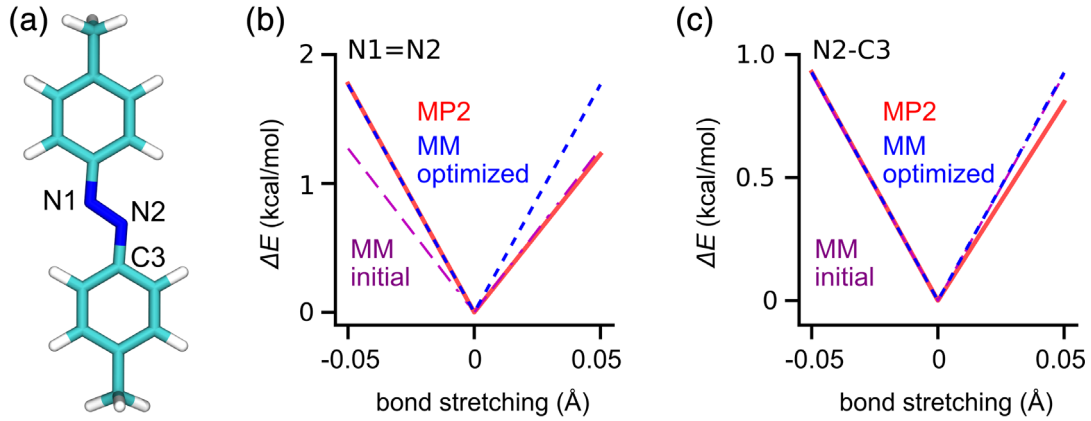

FIGURE 3 Three-point PES scans computed with MP2/6-31G* for *trans*-4dmAB. We used a step of 0.05 Å to compute PES for bond stretching. QM profiles computed with MP2 are colored red. MM profiles computed with the initial versus optimized CHARMM parameters are colored magenta and blue, respectively. (a) Molecular structure of *trans*-4dmAB. (b and c) PES computed for the stretching of the N1═N2 (panel b) and N2—C3 bonds (panel c) [Color figure can be viewed at wileyonlinelibrary.com]

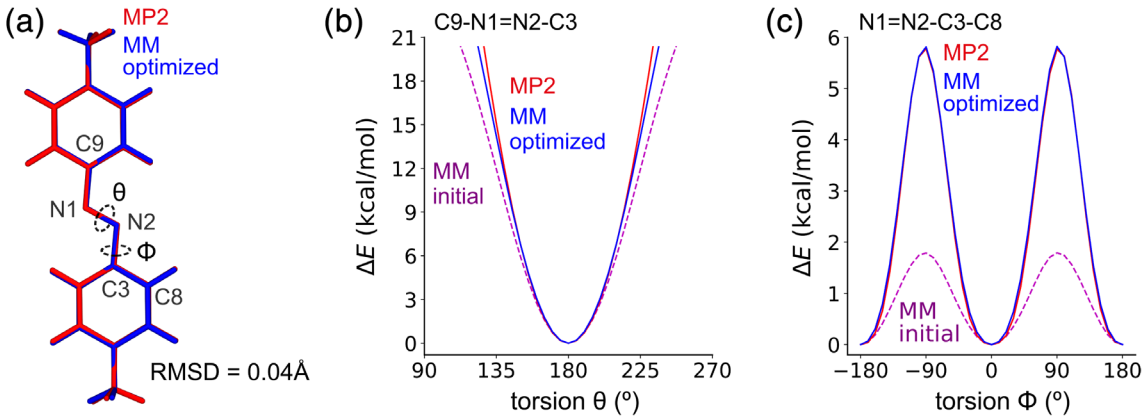

FIGURE 4 Optimization of bonded parameters for *trans*-4dmAB. (a) Overlap between MP2- and MM-optimized geometries for *trans*-4dmAB. (b) PES profile for the torsion around the N1═N2 bond. The MP2 energy profile is colored red; MM profiles obtained with the initial and optimized parameters are colored violet and blue, respectively. (c) Two-dimensional PES profile for the N1═N2 and N1—C3 rotations [Color figure can be viewed at wileyonlinelibrary.com]

The small tilt of ~2° between the two benzene rings in the starting crystal structure[4] is likely due to inter-molecular interactions in the crystal. From MM simulations with the parameters derived here, we obtained an average tilt angle of 3.5° (Table 5).

3.4 | Force-field description of FAAzo-4

We used the parameters optimized here for 4dmAB to prepare a set of parameters for FAAzo-4 in its *trans* and *cis* isomeric states. As in our parametrization protocol we used standard CGenFF partial atomic charges for the benzene ring atoms and for methyl group atoms, we could replace the two methyl groups by butane and butanoic acid groups, respectively. Parameters for buthane and butanoic acid are transferred from CGenFF. The force field parameters for FAAzo-4 are presented in the Supporting Information.

3.5 | Crystal lattice simulation of *trans*-4dmAB and *trans*-FAAzo-4

To test the parameters we derived for *trans*-4dmAB, we performed crystal lattice simulations for *trans*-4dmAB at 296 K, and for *trans*-FAAzo-4 at 100 K (Figures S1 and S2). The temperatures we chose are the same as used in crystallography.

Simulations of a crystal of 64 *trans*-FAAzo-4 molecules reproduced the size of the unit cell to within 0.3 Å with parameter Set-1, and to within 0.1 Å with Set-2 (Table 9, Figures S6 and S7). Similarly small errors were obtained in simulations of the *trans*-4dmAB crystal at room temperature (Table 9).

We found that bond lengths, angles (Table 5), and inter-molecular distances (Figures 5, S1c,d, and S2c,d) were accurately represented in the simulations. These computations, and the PES profiles discussed above, indicate that the parameters we derived here provide a reliable representation of *trans*-FAAzo-4.

3.6 | Optimization of bonded parameters for *cis*-4dmAB

In *cis*-4dmAB, two benzene rings are in close van der Waals contact (Figure 6), and test computations indicated that we could not accurately describe structural properties of *cis*-4dmAB with parameters derived above for *trans*-4dmAB. To improve the description of the structural properties of *cis*-4dmAB, we increased the force constants for N1═N2 and N2—C3 bonds relative to *trans*-4dmAB, and decreased force constants for valence angles N1═N2—C3 and N2—C3—C8 (Table 2, Figures 6 and S8).

Our tests for the parametrization of dihedral angles involving the central double bond of *cis*-4dmAB revealed that two helical

TABLE 9 Error in crystal lattice vectors computed from MM simulations of *trans*-FAAzo-4 and *trans*-4dmAB

Molecule	Temperature	Parameter set	Error in *a* (Å)	Error in *b* (Å)	Error in *c* (Å)	Sum of errors (Å)
FAAzo-4	100 K	MM initial	0.27	0.04	0.10	0.41
		Set-1	0.21	0.03	0.07	0.31
		Set-2	−0.09	−0.01	−0.03	−0.13
4dmAB	296 K	Set-1	0.14	0.06	0.12	0.32
		Set-2	0.05	0.02	0.04	0.10

Note: The error was computed as the difference between the length of the unit cell along the *a*, *b*, and *c* crystal lattice vectors in the crystal structure versus simulations. All computations were performed with 64 molecules in the unit cell of the crystal.

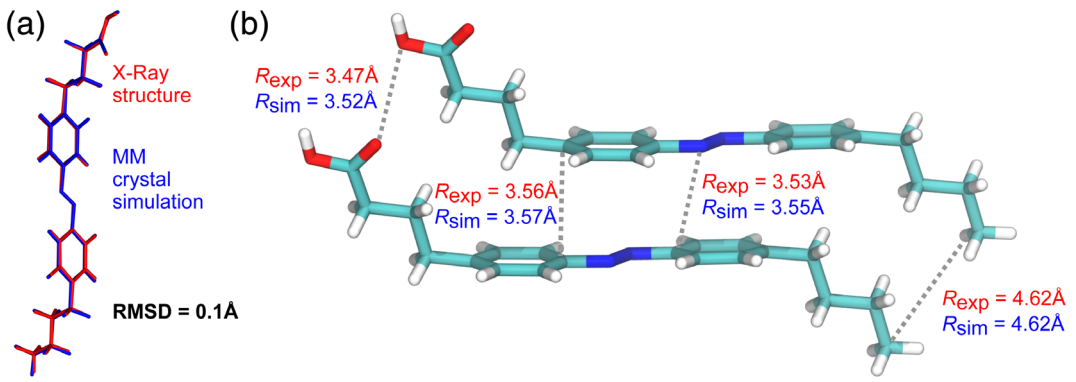

FIGURE 5 The parameters derived here allow good description of the structure of FAAzo-4. (a) MM crystal structure averaged from the simulation trajectory (blue) superimposed on X-ray crystal structure (red). (b) Stacking of FAAzo-4 molecules in the X-ray crystal structure. Intermolecular distances computed for X-ray structure and averaged from MD simulation are denoted in red and blue, respectively [Color figure can be viewed at wileyonlinelibrary.com]

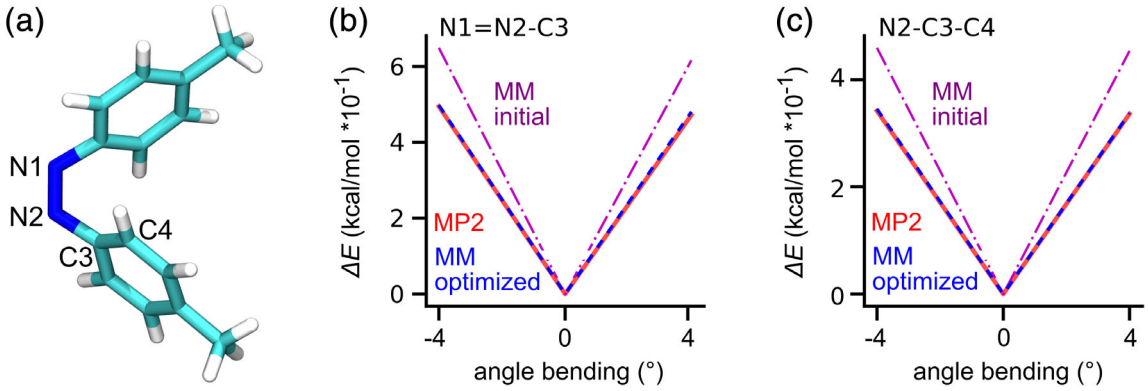

FIGURE 6 Three-point PES scans computed with MP2/6-31G* for *cis*-4dmAB. We used a step of 0.05 Å to compute PES for bond stretching. QM profiles computed with MP2 are colored red. MM profiles computed with the initial versus optimized CHARMM parameters are colored magenta and blue, respectively. (a) Molecular structure of *cis*-4dmAB. (b and c) PES computed for the bending of the N1═N2—C3 (panel b) and N2—C3—C4 bonds (panel c) [Color figure can be viewed at wileyonlinelibrary.com]

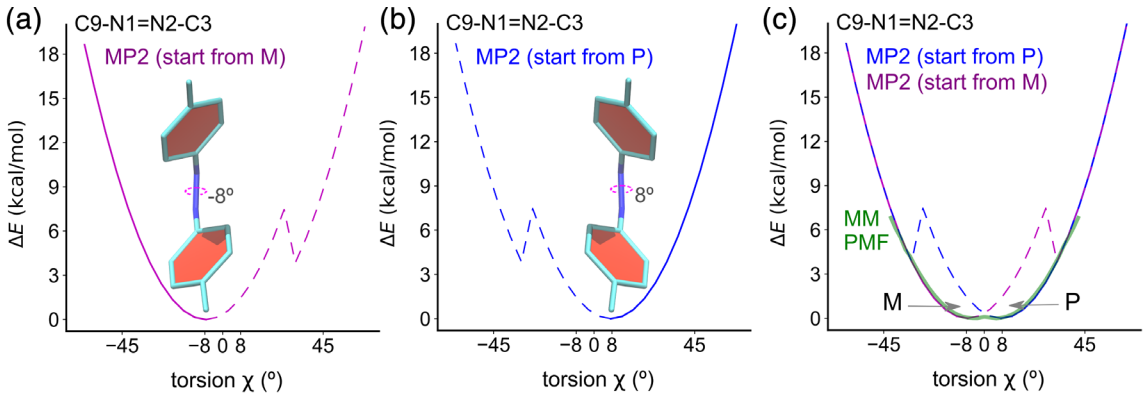

FIGURE 7 Resolving *cis*-4dmAB PES for C9—N1═N2—C3 dihedral angle in the region of M and P minima. (a) PES scan initiated from M enantiomer. (b) PES scan initiated from P enantiomer. (c) PES combined from scans presented in panels (a) and (b) [Color figure can be viewed at wileyonlinelibrary.com]

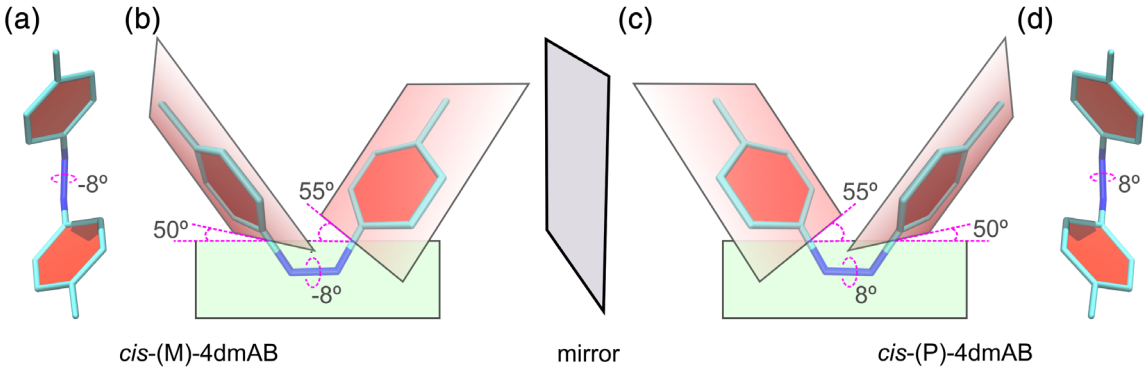

SCHEME 2 Helical chirality of *cis*-4dmAB. (a,b) Molecular graphics of *cis*-(M)-4dmAB. (c,d) Molecular graphics of *cis*-(M)-4dmAB. Red planes are parallel to the benzene rings. The green plane is drawn along the N1═N2 bond and is parallel to the page [Color figure can be viewed at wileyonlinelibrary.com]

enantiomers, *cis*-(M)-4dmAB and *cis*-(P)-4dmAB, have the same energy (Figure 7). These two enantiomers are distinguished by the twist around the central N1═N2 bond, which is 8° in *cis*-(P)-4dmAB and −8° in *cis*-(M)-4dmAB (Scheme 2). This difference in the bond twist associates with different relative orientation of the two benzene rings (Figures 8c and 9d). For simplicity, in what follows, we label the *cis*-(P)-4dmAB and *cis*-(M)-4dmAB as P and M, respectively.

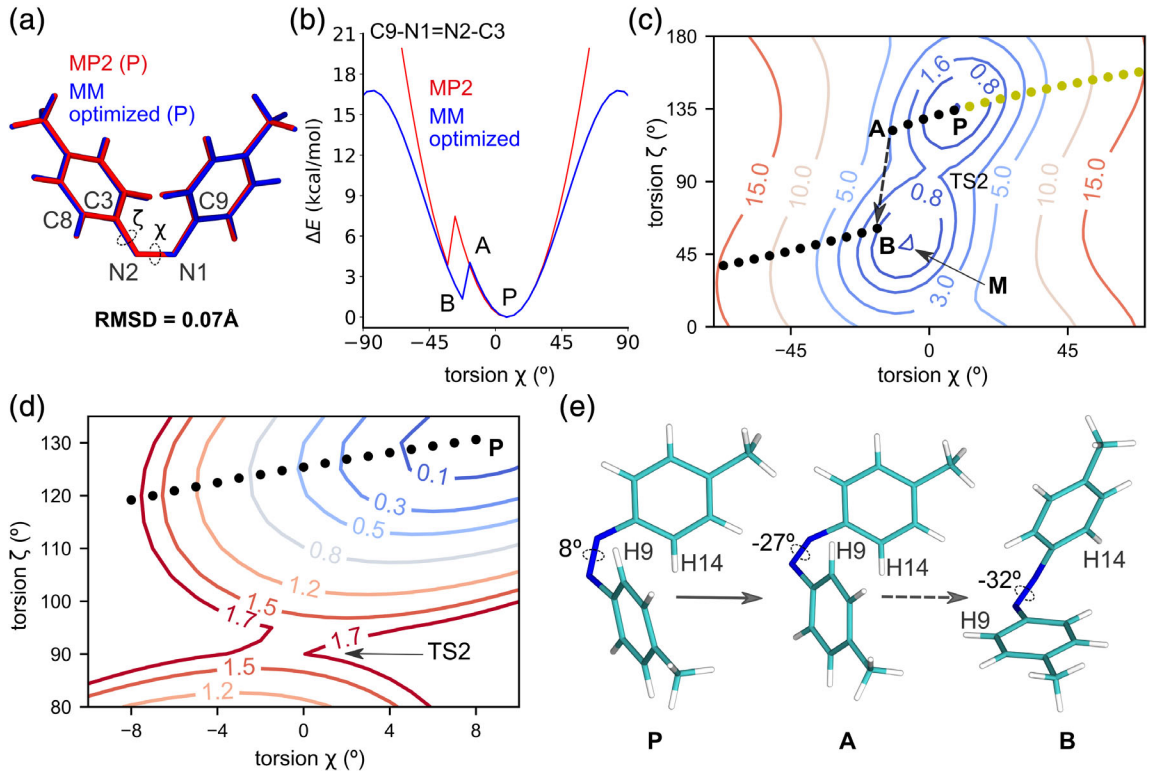

FIGURE 8 Optimization of bonded parameters for *cis*-4dmAB. (a) We compare the *cis*-4dmAB structures optimized with MP2 (red), and with the MM parameters derived here (blue). (b) PES profiles for twisting the N1═N2 bond. (c) Two-dimensional PES profile used to evaluate the discontinuity in the one-dimensional PES from panel (b). Black and yellow dots represent the bidirectional scan of the C9—N1═N2—C3 dihedral angle with decreasing and, respectively, increasing values of the angle. (d) Two-dimensional PES magnified in the region of TS2 and P minimum. (e) Structure of *cis*-4dmAB at points P, A, B illustrated in panels (b) and (c) [Color figure can be viewed at wileyonlinelibrary.com]

We computed the PES for the C3—N1═N2—C9 dihedral angle by twisting the N1═N2 bond counterclockwise starting from the M enantiomer, and clockwise starting from P. During both computations, the distance between the two benzene rings of *cis*-4dmAB increased; both PES profiles were continuous, that is, without discontinuities in energy values (solid lines in Figure 7a,b). By contrast, when we twisted the N1═N2 clockwise for M (counterclockwise for P), we obtained geometries in which the repulsion between hydrogen atoms of the two benzene rings gave rise to discontinuities in both of the PES profiles (dashed line in Figure 7a,b). Close inspection of the scans indicated that the P enantiomer is not visited when twisting clockwise from the M enantiomer; likewise, the M enantiomer is not visited when twisting counterclockwise from the P enantiomer.

To resolve discontinuities of the PES profiles, we combined the PES computations started from M and P minima, and used the combined profile to resolve the shape of the minima at −8° and 8° (Figure 7c). The PES profile for the C9—N1═N2—C3 dihedral angle (χ in Figure 7c) is now continuous in the region of the M and P enantiomers.

At minima on the combined PES, the N1═N2—C3—C8 dihedral angle (Figure 8a) is −55° or 130° for the P enantiomer, as compared to 55° or −130° for the M enantiomer (see ζ angle in Figure 9d). The profile for the N2—C3 bond twist has two transition states close to χ = 0 (Figure 9): TS1 (3.8 kcal/mol above M) occurs at ζ = 0° and ζ = −180°; TS2 (1.6 kcal/mol above M) occurs at ζ = 90° and ζ = −90° (Figure 9d).

To further investigate torsions at the central region of *cis*-4dmAB, we computed two-dimensional MM PES profiles for the χ and ζ dihedral angles. As illustrated in Figure 9b, M and P are close to each other in this two-dimensional PES, being separated by a very narrow transition state (TS2) with an energy barrier of 1.7 kcal/mol relative to M. In the one-dimensional PES scan for the χ dihedral angle (Figure 8b), TS2 is not sampled when the χ dihedral angle is 0°; instead, from the P enantiomer *cis*-4dmAB goes to A (χ = −27°) and then directly to B (χ = −32°) without visiting the M minimum at χ = 8° (Figure 8c).

In the one-dimensional PES for ζ, TS2 is sampled and its energy is the same, 1.7 kcal/mol, as that of TS2 in the two-dimensional PES. In the case of the ζ dihedral angle (Figure 9a), we could reproduce with MM the QM energy for TS1; for TS2, the MM and QM values agreed to within 1 kcal/mol (Figure 9a).

The MM-optimized structure of *cis*-4dmAB agrees well with the crystal structure of *cis*-azobenzene from Mostad and Rømming[27] (Table 6) and with the MP2-optimized structure (RMSD = 0.07 Å between MP2 and MM). In the MP2-optimized structure and in the crystal structure,[27] the central N1═N2 bond is twisted by ∼8°. We obtained overall good agreement between MM with MP2 target

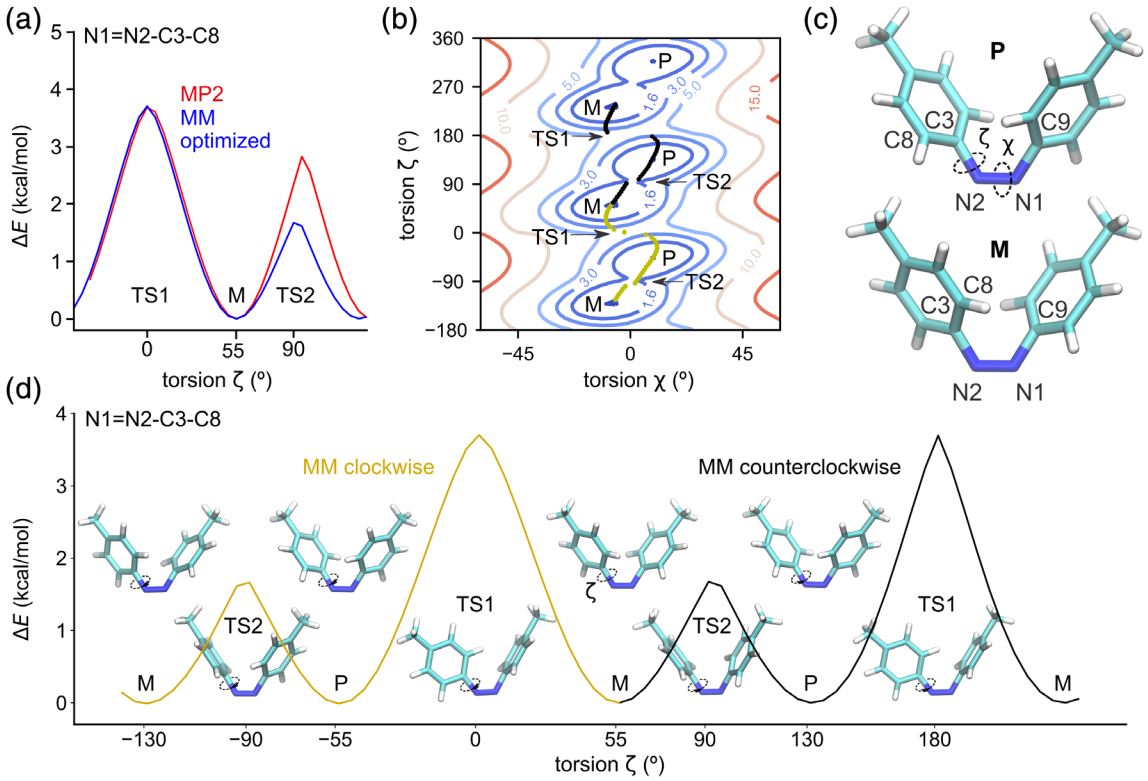

FIGURE 9 Optimization of bonded parameters for *cis*-4dmAB. (a) MP2 (red) and MM PES profile (blue) for twisting the N2—C3 bond. (b) PES profiles for torsions around the N1═N2 and N2—C3 bonds. The two-dimensional PES indicates that the one-dimensional PES from panel b follows the minimum energy path. Black dots represent the part of bidirectional scan with decreasing values of N1═N2—C3—C8 dihedral angle. Yellow dots represent part of a scan with increasing values of N1═N2—C3—C8 dihedral angle. (c) P and M enantiomers of *cis*-4dmAB. (d) MM PES scan of 360° for N1═N2—C3—C8 dihedral angle [Color figure can be viewed at wileyonlinelibrary.com]

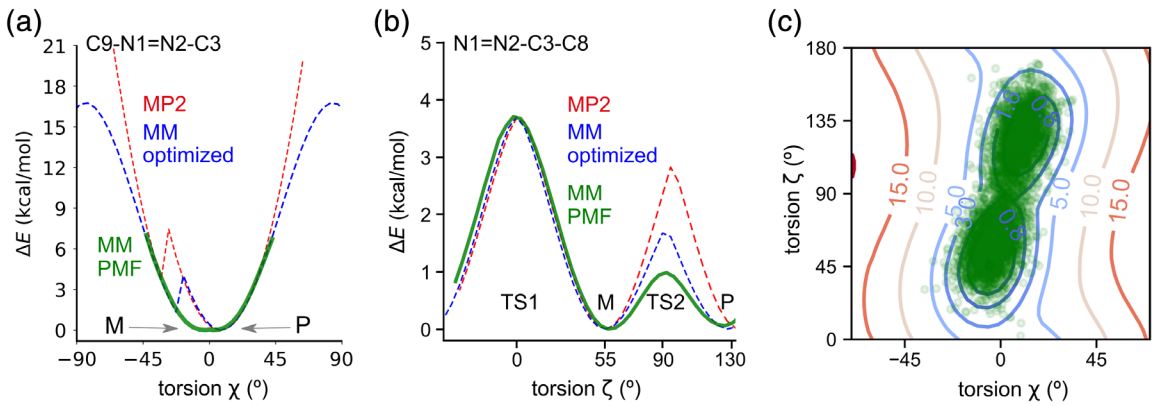

FIGURE 10 MM PMF profiles for *cis*-4dmAB torsions. (a) PMF profile for N1═N2 torsion. (b) PMF profile for N2—C3 torsion. (c) Sampling of the dihedral angle in molecular dynamics simulations at room temperature [Color figure can be viewed at wileyonlinelibrary.com]

values for bond stretching, angle bending (Figures 6 and S8), and torsional profiles (Figures 8b, 9a, and S9).

An exception is the energy of the TS2 intermediate relative to the M enantiomer: relative to the value computed with one-dimensional MP2 PES, values obtained from one-dimensional MM PES or MM PMF computations are lower by ~1 kcal/mol and ~2 kcal/mol, respectively (Figures 9a and 10b). This discrepancy between the one-dimensional MM profiles in the region of TS2 suggest that, at this region of the PES, degrees of freedom other than the C9—N1═N2—C3 dihedral angle might contribute to the reaction coordinate between the M and P enantiomers of *cis*-4dmAB.

Inspection of the two-dimensional MM PES indicated that at TS2 the C9—N1═N2—C3 (χ in Figures 8d and 9b) is 0°, and N1═N2—C3—C8 (χ in Figures 8d and 9b) is 90°. Values of PMF for χ, ζ one-dimensional PMF profiles at χ = 0 have somewhat different values, 0.1 kcal/mol versus 1 kcal/mol, respectively (Figure 10a,b).

TABLE 10 Energy difference between the *cis* and *trans* isomers of 4dmAB computed with the MM-optimized parameters versus QM

Method	$\Delta E = E_{cis} - E_{trans}$ (kcal/mol)
B3LYP/6-31G**	15.5
MP2/6-31G*	11.8
MM	19.6

In the corresponding one-dimensional PES for ζ, TS2 is sampled when starting from the either M or P enantiomers. TS2 is not sampled in the one-dimensional profile of χ (Figure 8c) and further tests indicated that in the two-dimensional PES starting from P, a conformer with $\chi = 0^\circ$ can be reached without visiting TS2, and with an energy cost as low as 0.5 kcal/mol (Figure 8d). This could explain why the PMF profile indicates sampling of conformers with $\chi = 0^\circ$ at a relatively low energetic cost of ~0.1 kcal/mol.

At the MP2/6-31G* level of theory used for the parametrization, *cis*-4dmAB is 11.8 kcal/mol higher in energy than *trans*-4dmAB; with B3LYP, the energy difference is 15.5 kcal/mol (Table 10). The somewhat higher energy difference indicated by B3LYP likely originates from the overestimation of electron delocalization in *trans*-4dmAB. The MM parameters we derived give a reasonable description of the energy difference between *cis*- and *trans*-4dmAB; the 20 kcal/mol MM energy difference arises from N1═N2, N2—C3 bond and C9—N1═N2—C3, N1═N2—C3—C8 dihedral force constants being raised for *cis*-4dmAB with respect to *trans*-4dmAB parameters.

3.7 | MM simulations and PMF computations of *cis*-4dmAB

The challenges we encountered when parametrizing dihedral angle terms for *cis*-4dmAB prompted us to use MM simulations to evaluate the dynamics of bond twists in the central region of *cis*-4dmAB. From the simulation trajectory of *cis*-4dmAB at 300 K, we first extracted the values of the dihedral angles for six dihedral angles of *cis*-4dmAB (Figure S9), and used Equation (3) to calculate PMF profiles for each of these dihedral angles. As summarized in Figures 10 and S9, the PES profiles indicate proper sampling of the dihedral angle values close to equilibrium, without any of the discontinuities observed in PES profiles.

The small barrier observed in the one-dimensional PES for the C9—N1═N2—C3 dihedral angle of *cis*-4dmAB is absent in simulations at room temperature. Importantly, during independent MD simulations in which we started from *cis*-(M)-4dmAB or *cis*-(P)-4dmAB we observed that both the *cis*-(P)-4dmAB and *cis*-(M)-4dmAB enantiomers are sampled (Figures 10C and S10). Pursuant to these test computations, we suggest that the parameters derived here provide a good description of the dynamics of *cis*-4dmAB in equilibrium simulations at room temperature.

4 | CONCLUSIONS

The molecular picture of how photo-switchable lipids interact with other lipid species within the membrane environment is largely unclear. Open questions include the location of the photo-switchable lipids in lipid bilayers, how photo-switchable lipids interact with each other and with other components of the membrane (lipid molecules, water at the membrane interface, proteins), and how isomerization impacts the molecular interactions of the photo-switchable lipids. We presented here force field parameters for the photo-switchable fatty acid FAAZo-4 in *trans* and *cis* conformations.

To ensure the compatibility of the FAAzo-4 parameters with the CHARMM parameters for lipids and proteins, we used the CGenFF protocol for the parametrization of drug-like molecules.[21] The parameters we derived allow good description of the geometry and torsional properties of FAAzo-4. In molecular dynamics simulations of crystals, we obtain good agreement with X-ray diffraction data for the dimensions of the unit cells, molecular structure, and intermolecular distances (Tables 5, 9, Figures 5, S1 and S2).

The parametrization of the partial atomic charges was performed using *cis*-4dmAB, as for this conformer we could sample all sites in water interaction energy computations.

The partial atomic charges of *cis*-4dmAB allowed reliable parametrization of *trans*-4dmAB, including of the torsional profiles for the central double bond region (Figure 4). Parametrization of the torsional profiles for dihedral angles involving the central N1═N2 double bond of *cis*-4dmAB was challenging due to the presence of the *cis*-(M)-4dmAB and *cis*-(P)-4dmAB enantiomers being separated by a low-energy barrier (Figure 8c) that was difficult to describe with one-dimensional PES scans. To circumvent this issue, we used two-dimensional PES scans to probe the reaction path between the M and P enantiomers. We then computed PMF profiles for selected dihedral angles to verify that, at room temperature, the energy profile for interconversions between the M and P enantiomers of *cis*-(M)-4dmAB is smooth, without any discontinuities (Figures 10 and S9).

The profiles for the water interaction energies of the central double bond for *trans*-4dmAB versus *cis*-4dmAB (Figure 2) indicate that the *cis* photo-switchable lipid has stronger, that is, energetically more favorable water interactions than the *trans* lipid. Based on this result, we speculate that the *trans* photo-switchable lipid might locate deeper into the membrane plane than the *cis* lipid, whose double bond might rather prefer interactions closer to the lipid headgroup interface of the lipid bilayer.

The parameters derived here for the azobenzene moiety can be transferred to describe azobenzene-containing lipids for applications in photo-pharmacology—such as photo-switchable phosphatidylcholine,[6] diacylglycerol,[42] and ceramide.[10] As the parameters were derived using the CGenFF protocol for drug-like compounds, we suggest that they are applicable for simulations to probe, for example, the response of a lipid membrane to the presence of a small number of photo-switchable lipids, or the binding of a photo-switchable lipid to an ion channel. Atomistic models of lipid bilayers with high concentrations of

photo-switchable lipids will likely require further developments from experiments and force-field parametrizations.

ACKNOWLEDGMENTS

Research was funded in part by the German Research Foundation (DFG) Priority Research Program SPP1926 (to A-NB and DT) and by the Freie Universität Berlin within the Excellence Initiative of the German Research Foundation (to A-NB). Computations were performed using the Soroban supercomputer cluster of the ZEDAT Freie Universität Berlin, and on the computer cluster of the Department of Physics of the Freie Universität Berlin. We thank Jens Dreger and the ZEDAT team for excellent technical support. We acknowledge the usage of parametrization scripts from the webpage of Prof. MacKerell at the University of Maryland. Open access funding enabled and organized by Projekt DEAL.

AUTHOR CONTRIBUTIONS

Oskar Klaja: Performed all computations, prepared figures and files for the force-field parameters presented here. **James Frank** and **Dirk Trauner:** Provided crystal structure coordinates and contributed to data interpretation. **Ana-Nicoleta Bondar:** Designed and supervised the project. **Oskar Klaja** and **Ana-Nicoleta Bondar:** Wrote the manuscript with input from **James Frank** and **Dirk Trauner**.

ORCID

Oskar Klaja https://orcid.org/0000-0001-6635-8097
James A. Frank https://orcid.org/0000-0001-6705-2540
Dirk Trauner https://orcid.org/0000-0002-6782-6056
Ana-Nicoleta Bondar https://orcid.org/0000-0003-2636-9773

REFERENCES

[1] J. Broichagen, J. A. Frank, D. Trauner, *Acc. Chem. Res.* **2015**, *48*, 1947.
[2] L. Laprell, I. Tochitsky, K. Kaur, M. B. Manookin, M. Stein, D. M. Barber, C. Schön, S. Michalakis, M. VBiel, R. H. Kramer, M. P. Sumser, D. Trauner, R. N. Van Gelder, *J. Clin. Invest.* **2017**, *127*, 2598.
[3] J. Broichagen, M. Schönberger, S. C. Cork, J. A. Frank, P. Marchetti, M. Bugliani, A. M. J. Shapiro, S. Trapp, G. A. Rutter, D. J. Hodson, D. Trauner, *Nat. Commun.* **2014**, *5*, 5116.
[4] J. A. Frank, M. Moroni, R. Moshourab, M. Sumser, G. R. Lewin, D. Trauner, *Nat. Commun.* **2015**, *6*, 7118.
[5] J. H. A. Folgering, J. M. Kuiper, A. H. de Vries, J. B. F. N. Engberts, B. Poolman, *Langmuir* **2004**, *20*, 6985.
[6] C. Pernpeintner, J. A. Frank, P. Urban, C. R. Roescke, S. D. Pritzk, D. Trauner, T. Lohmüller, *Langmuir* **2017**, *33*, 4083.
[7] P. Urban, S. D. Pritzk, D. B. Konrad, J. A. Frank, C. Pernpeintner, C. R. Roescke, D. Trauner, T. Lohmüller, *Langmuir* **2018**, *34*, 13368.
[8] B. R. Brooks, R. E. Bruccoleri, B. D. Olafson, D. J. States, S. Swaminathan, M. Karplus, *J. Comput. Chem.* **1983**, *4*, 187.
[9] H. Fliegl, A. Köhn, C. Hätting, R. Ahlrichs, *J. Am. Chem. Soc.* **2003**, *125*, 9821.
[10] J. A. Frank, H. G. Franquelin, P. Schwille, D. Trauner, *J. Am. Chem. Soc.* **2016**, *138*, 12981.
[11] A. K. Rappé, C. J. Casewit, K. S. Colwell, W. A. Goddard III., M. A. Skiff, *J. Am. Chem. Soc.* **1992**, *114*, 10024.
[12] H. Sun, S. J. Mumby, J. R. Maple, A. T. Hagler, *J. Am. Chem. Soc.* **1994**, *116*, 2978.
[13] H. Sun, *J. Phys. Chem. B.* **1998**, *102*, 7338.
[14] Z. Li, P. Wang, B. Liu, Y. Wang, J. Zhang, Y. Yan, Y. Ma, *Soft Matter* **2014**, *10*, 8758.
[15] Y. Li, B. Hartlke, *J. Chem. Phys.* **2013**, *139*, 224303.
[16] X. Zheng, D. Wang, Z. Shuai, X. Zhang, *J. Phys. Chem. B.* **2012**, *116*, 823.
[17] P. Duchstein, C. Neiss, A. Görling, D. Zahn, *J. Mol. Model.* **2012**, *18*, 2479.
[18] G. Tiberio, L. Muccioli, R. Berardi, C. Zannoni, *ChemPhysChem* **2010**, *11*, 1018.
[19] M. McCullagh, I. Franco, M. A. Ratner, G. C. Schatz, *J. Am. Chem. Soc.* **2011**, *133*, 3452.
[20] M. McCullagh, I. Franco, M. A. Ratner, G. C. Schatz, *J. Phys. Chem. Lett.* **2012**, *4*, 689.
[21] K. Vanommeslaeghe, E. Hatcher, C. Acharya, S. Kundu, S. Zhong, J. Shim, E. Darian, O. Guvench, P. Lopes, I. Vorobyov, A. D. MacKerell Jr., *J. Comput. Chem.* **2010**, *31*, 671.
[22] A. D. MacKerell Jr., M. Feig, C. L. I. Brooks, *J. Comput. Chem.* **2004**, *25*, 1400.
[23] W. L. Jorgensen, J. Chandrasekhar, J. D. Madura, R. W. Impey, M. L. Klein, *J. Chem. Phys.* **1983**, *79*, 926.
[24] K. Vanommenslaeghe, A. D. MacKerell Jr., *J. Chem. Inf. Model.* **2012**, *52*, 3144.
[25] M. D. Hanwell, D. E. Curtis, D. C. Lonie, T. Vandermeersch, E. Zurek, G. R. Hutchison, *Aust. J. Chem.* **2012**, *4*, 17.
[26] G. Schaftenaar, J. H. Noordik, *J. Comput. Aid. Mol. Des.* **2000**, *14*, 123.
[27] A. Mostad, C. Rømming, *Acta Cryst. Scandin.* **1971**, *25*, 3561.
[28] M. J. Frisch, G. W. Trucks, H. B. Schlegel, G. E. Scuseria, M. A. Robb, J. R. Cheeseman, G. Scalmani, V. Barone, B. Mennucci, G. A. Petersson, H. Nakatsuji, M. Caricato, X. Li, H. P. Hratchian, A. F. Izmaylov, J. Bloino, G. Zheng, J. L. Sonnenberg, M. Hada, M. Ehara, K. Toyota, R. Fukuda, J. Hasegawa, M. Ishida, T. Nakajima, Y. Honda, O. Kitao, H. Nakai, T. Vreven, J. A. Montgomery Jr., J. E. Peralta, F. Pogliaro, M. Beapark, J. J. Heyd, E. Brothers, K. N. Kudin, V. N. Staroverov, T. Keith, R. Kobayashi, J. Normand, K. Raghavachari, A. Rendell, J. C. Burant, S. S. Iyengar, J. Tomasi, M. Cossi, N. Rega, J. M. Millam, M. Klene, J. E. Knox, J. B. Cross, V. Bakken, C. Adamo, J. Jaramillo, R. Gomperts, R. E. Stratmann, O. Yazyev, A. J. Austin, R. Cammi, C. Pomelli, J. W. Ochterski, R. L. Martin, K. Morokuma, V. G. Zakrzewski, G. A. Voth, P. Salvador, J. J. Dannenberg, S. Dapprich, A. D. Daniels, O. Farkas, J. B. Foresman, J. V. Ortiz, J. Ciosliwski, D. J. Fox Gaussian, Inc., Wallingford CT, **2013**.
[29] C. G. Mayne, J. Saam, K. Schulten, E. Tajkhorshid, J. C. Gumbart, *J. Comput. Chem.* **2013**, *34*, 2757.
[30] W. Humphrey, W. Dalke, K. Schulten, *J. Mol. Graph.* **1996**, *14*, 33.
[31] D. Kraft Tech. Rep. *DFVLR-FB 88-28*, DLR German Aerospace Center - Institute for Flight Mechanics, Köln, Germany **1988**.
[32] K. Vanommeslaeghe, M. Yang, A. D. MacKerell Jr., *J. Comput. Chem.* **2015**, *36*, 1083.
[33] C. F. Macrae, I. J. Bruno, J. A. Chisholm, P. R. Edgington, P. McCabe, E. Pidcock, L. Rodriguesz-Monge, R. Taylor, J. van de Streek, P. A. Wood, *J. Appl. Crystallogr.* **2008**, *41*, 466.
[34] L. Kalé, R. Skeel, M. Bhandarkar, R. Brunner, A. Gursoy, N. Krawetz, J. Phillips, A. Shinozaki, K. Varadarajan, K. Schulten, *J. Comput. Phys.* **1999**, *151*, 283.
[35] J. C. Phillips, B. Braun, W. Wang, J. Gumbart, E. Takjkhorshid, E. Villa, C. Chipot, R. D. Skeel, L. Kale, K. Schulten, *J. Comput. Chem.* **2005**, *26*, 1781.
[36] A. Nemkevich, H.-B. Bürgi, M. A. Spackman, B. Corry, *Phys. Chem. Chem. Phys.* **2010**, *12*, 14916.
[37] T. Darden, D. York, L. Pedersen, *J. Chem. Phys.* **1993**, *98*, 10089.
[38] U. Essmann, L. Perera, M. L. Berkowitz, T. Darden, H. Lee, L. G. Pedersen, *J. Chem. Phys.* **1995**, *103*, 8577.
[39] J. Harada, K. Okawa, S. Tomoda, *Acta Cryst.* **1997**, B53, *53*, 662.
[40] J. A. Bouwstra, A. Schouten, J. Kroon, *Acta Cryst.* **1983**, *C39*, 1121.
[41] M. Böckmann, N. L. Doltsinis, D. Marx, *J. Phys. Chem. A* **2010**, *114*, 745.

[42] J. A. Frank, D. A. Yuschchenko, D. J. Hodson, N. Lipstein, J. Nagpal, G. A. Rutter, J.-S. Rhee, A. Gottschalk, N. Brose, C. Schultz, D. Trauner, *Nat. Chem. Biol.* **2016**, *12*, 755.

SUPPORTING INFORMATION

Additional supporting information may be found online in the Supporting Information section at the end of this article.

How to cite this article: Klaja O, Frank JA, Trauner D, Bondar A-N. Potential energy function for a photo-switchable lipid molecule. *J Comput Chem*. 2020;41:2336–2351. https://doi.org/10.1002/jcc.26387